Provided for non-commercial research and education use.
Not for reproduction, distribution or commercial use.

This article appeared in a journal published by Elsevier. The attached copy is furnished to the author for internal non-commercial research and education use, including for instruction at the authors institution and sharing with colleagues.

Other uses, including reproduction and distribution, or selling or licensing copies, or posting to personal, institutional or third party websites are prohibited.

In most cases authors are permitted to post their version of the article (e.g. in Word or Tex form) to their personal website or institutional repository. Authors requiring further information regarding Elsevier's archiving and manuscript policies are encouraged to visit:

http://www.elsevier.com/copyright

Author's personal copy

Combustion and Flame 156 (2009) 1014–1022

Contents lists available at ScienceDirect

Combustion and Flame

www.elsevier.com/locate/combustflame

Chemical speciation of premixed ethylbenzene flames at the soot onset limit at various (ϕ, T) pairs

Ali Ergut [a], Rick J. Therrien [a], Yiannis A. Levendis [a,*], Henning Richter [b], Jack B. Howard [b], Joel B. Carlson [c]

[a] Department of Mechanical and Industrial Engineering, Northeastern University, Boston, MA 02115, USA
[b] Department of Chemical Engineering, Massachusetts Institute of Technology, Cambridge, MA 02139, USA
[c] US Army SBCCOM – Natick Soldier Center, Natick, MA 01760, USA

ARTICLE INFO

Article history:
Received 22 July 2008
Received in revised form 16 October 2008
Accepted 11 November 2008
Available online 25 December 2008

Keywords:
Premixed combustion
One-dimensional flame
Ethylbenzene
PAH
Soot onset

ABSTRACT

This work investigates the similarities/differences of one-dimensional, laminar, atmospheric pressure premixed ethylbenzene flames at their soot onset threshold (ϕ_{critical}). The goals of this investigation are to contrast the entire temperature profiles of the flames at various critical equivalence ratios, ϕ_{critical}, and to report on hydrocarbon specie profiles. Liquid ethylbenzene was pre-vaporized in nitrogen, blended with an oxygen–nitrogen mixture and, upon ignition, premixed flat flames were stabilized over a burner at atmospheric pressure. The C/O ratio was regulated and simultaneously the temperature profile was adjusted by varying the heat lost from the flame to the burner, to obtain visually similar flames, all at their apparent soot onset limit. Temperature profiles of five such flames were determined with thermocouples. The results indicate that as the axial temperature profiles in the flames rose, ϕ_{critical} ($(\text{C/O})_{\text{critical}}$) also increased. Sampling was performed at various heights along the axes of three of these flames ($\phi_{c1} = 1.68$, $\phi_{c2} = 1.74$ and $\phi_{c3} = 1.83$) to monitor changes in chemical speciation. The mole fractions of CO increased in the order of increasing equivalence ratio and hence increasing flame temperature. The CO_2 mole fractions of the three flames were similar. However, the mole fractions of light hydrocarbons and polycyclic aromatic hydrocarbons (PAH), which are suspected soot precursors, decreased in the order of increasing equivalence ratio and hence increasing flame temperature. Whereas direct measurements of particulate matter in the flame were not made in this work, these observations on soot precursors along with theoretical flame emissivity considerations suggest that particulate loadings at the sooting limit also decreased in the order of increasing equivalence ratio and hence increasing flame temperature.

© 2008 The Combustion Institute. Published by Elsevier Inc. All rights reserved.

1. Introduction

To minimize soot emissions from combustion sources, a clear understanding of the factors governing the propensity to form soot is required. The fuel molecular structure, along with flame temperature, fuel/oxidizer ratio, gas dynamics of the system and pressure are influential parameters that determine the threshold and quantity of soot formed in a given flame.

In burner type combustion systems, however, it is difficult to separate the effect of the equivalence ratio (ϕ) from that of the temperature (T), since temperature is a function of equivalence ratio among other parameters. To investigate the effects of ϕ and temperature independently from each other, two studies were recently conducted in this laboratory: (i) on the effect of ϕ on the soot onset chemistry at constant T [1], and (ii) on the effect of T on the soot onset chemistry at constant ϕ [2], both involving atmospheric pressure ethylbenzene flames. The results indicate that the soot onset limit depends on both T and ϕ, both having independent effects on the flame chemistry. Within the investigated parameter range: ($1.68 \leqslant \phi \leqslant 1.83$) [1] and ($1826\ \text{K} \leqslant T_{\max} \leqslant 1921\ \text{K}$) [2], temperature was found to be more influential in affecting the chemical compositions of species.

The effects of temperature and ϕ on soot onset in flat flames have also been investigated by others and detailed literature reviews can be found in [1,2]. Based on experiments involving various fuels, a wide range of flame conditions, and various measurement techniques [3–9], it is widely accepted that the measured flame temperature increases in parallel to the critical equivalence ratio, ϕ_c, defined as the ratio of the actual fuel/air (or oxygen) mass ratio to stoichiometric fuel/air (oxygen) mass ratio where incipient soot is visually first detected as a faint orange glow in the flame.

Markatou et al. [10] investigated the onset of sooting in laminar, premixed flames of ethane, ethylene and acetylene computationally. They compared their computed ϕ_c with the experimentally derived ϕ_c values of Harris et al. [8]. Their analysis suggested that the appearance of soot is controlled by two factors, the concen-

[redacted]

0010-2180/$ – see front matter © 2008 The Combustion Institute. Published by Elsevier Inc. All rights reserved.
doi:10.1016/j.combustflame.2008.11.013

Author's personal copy

tration of acetylene and the growth of polycyclic aromatics. The latter is limited by rising flame temperatures towards the end of the main reaction zone. They also suggested that the beginning of the presence of soot particles, hence the sooting limit, is determined by particle nucleation not by subsequent particle growth or oxidation. Finally, they claimed that the dependence of the critical equivalence ratio on temperature may be partly explained on the basis of the reversibility of reaction steps leading to the formation and growth of PAH.

The present experimental research investigates the concentrations of individual fixed gases (CO, CO_2, O_2), light hydrocarbons (C_1–C_4 hydrocarbons and 1 ring aromatics), PAH and oxygenated species at the high-temperature soot onset threshold, as defined by Böhm et al. [7]. The relationship of temperature and ϕ_c is examined for atmospheric pressure premixed ethylbenzene flames. Rather than comparing the temperatures in one location in the post-flame regions of the different flames as Olson and Madronich [6], Böhm et al. [7] and Harris et al. [8] did, this work compares the entire measured temperature profiles of the flames, all at their soot onset limit [11]. The flames herein were selected as follows: In recent work [1], three flames with similar temperature profiles but different ϕ were investigated. One of these flames ($\phi = 1.74$) was at the soot onset limit; this flame was included in this work. The other two flames of Ref. [1] were either non-sooting ($\phi = 1.68$) or slightly sooting ($\phi = 1.83$). Herein, the temperature of the aforementioned non-sooting flame ($\phi = 1.68$) was lowered, by simply reducing its cold gas velocity through the burner, hence increasing the heat lost from the flame to the burner, until the flame appeared to be at the soot onset limit. This became the second flame of this study. Similarly, the temperature of the slightly sooting flame of previous study ($\phi = 1.83$) was raised, by increasing its cold gas velocity until its soot onset limit was reached. This became the third flame of this study. The mole fractions of fixed gases and hydrocarbon species in the resulting three flames, all at their soot onset limit ($\phi_c = 1.68$, 1.74 and 1.83), were contrasted. Two more flames with ϕ_c in-between the above mentioned were also established ($\phi_c = 1.71$ and 1.78) to better define the (ϕ_c, T) domain, and their temperature profiles were measured but sampling was not conducted for these two flames.

2. Experimental apparatus and procedure

Atmospheric pressure, premixed, laminar flat-flames were stabilized on a 50.8 mm diameter sintered bronze burner, Fig. 1. The burner temperature was controlled with air flowing through embedded copper tubing. Flames were isolated from the ambient air by a concentric sheath flow of N_2. The cold gas velocity of the sheath gas was 5.30 cm/s. Flames were stabilized with a perforated plate, positioned 30 mm from the burner surface and water-cooled with a copper coil. Liquid ethylbenzene (from *Fisher Scientific/Aldrich*), placed in two 50 mL glass syringes (*Hamilton*) and driven by a dual infusion/withdrawal syringe pump (*World Precision Instruments Inc.*), was introduced to a stainless-steel vaporizer (2 liters in volume) equipped with a nitrogen-flow-assisted atomizer. The vaporized fuel–nitrogen mixture was introduced to the bottom of the burner, through heated tubing, and it was mixed with a preheated oxidizing gas mixture (50 vol% O_2–50 vol% N_2). The vaporizer and the tubing were heated to a temperature, 20–50 °C higher than the boiling point of ethylbenzene, which is 137 °C. The ensuing mixtures are presented in Table 1. The temperature profiles of all five flames were determined via thermocouple measurements. All experiments were repeated in triplicate to analyze the sensitivity and repeatability of both temperature and species concentration measurements. Based on readings from flowmeters (pre-calibrated rotameters and mass flowmeters) the equivalence ratios during each of the tests were within ±0.05 of the aforementioned average values.

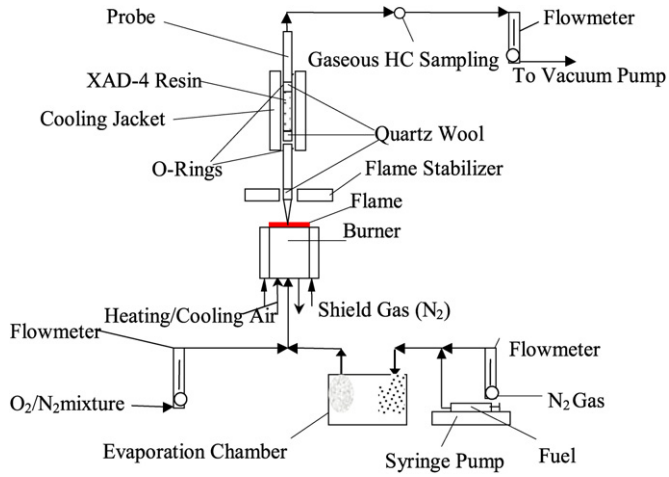

Fig. 1. One-dimensional burner and sampling set up.

Table 1
The compositions of five 1-D, atmospheric pressure, premixed ethylbenzene flames at soot onset limit. Fixed gases and hydrocarbon species were reported only for the flames in bold case, i.e. $\phi_c = 1.68$, $\phi_c = 1.74$ and $\phi_c = 1.83$.

ϕ_c	$(C/O)_c$	Ethylbenzene mole fraction	O_2 mole fraction	N_2 mole fraction	Cold gas velocity, cm/s
1.68	**0.641**	**0.040**	**0.253**	**0.707**	**6.92**
1.71	0.652	0.043	0.262	0.695	7.72
1.74	**0.664**	**0.047**	**0.284**	**0.669**	**7.81**
1.78	0.676	0.047	0.276	0.678	8.75
1.83	**0.691**	**0.051**	**0.293**	**0.656**	**10.17**

A 1-cm i.d. cooled quartz probe, with a tip diameter of 4.4 mm was used to sample combustion products at various heights inside three of the five flames. The reason that the probe's orifice was fairly large is that the same probe was used in previous studies [1,2,29], and particularly one of the flames studied [29] was highly sooting and smaller diameter orifice probes clogged during sampling. To be consistent with previous studies, the same probe was also used herein. Moreover, unlike studies elsewhere on gaseous fuels supplied to the burner by laboratory cylinders allowing long durations of experiments and thus long sampling times, the duration of the experiments herein were limited to 15 or 20 min. This time limitation was dictated by the size of the two 50 mL syringes loaded with liquid fuel and the necessary fuel flow rates in the range of 1.77–3.13 mL/min. Therefore, to collect sufficient amounts of sample for trace component analysis (PAH are trace components in these flames in the order of parts per billion) this larger probe orifice size was deemed (and proved to be) necessary. To minimize the disturbance of the flow field, sampling was performed *iso-axially* and *iso-kinetically*. Please note that the targeted flow rates in the sampling probe that correspond to iso-kinetic conditions at its orifice were determined based on the experimental temperature profile of each flame, which was measured first. For all cases, the resulting flowrate ratio of the burner gases to the sampled gases in the probe was 133/1, at flame temperatures. Furthermore, to minimize disturbance of the temperature field, the quartz probe was kept in the flame prior to sampling for a time sufficiently long to allow its tip to reach thermal equilibrium in the flame. Please note that the softening point of quartz has been reported to be 1938 K [12] and the maximum temperature in these flames was recorded to be 1920 K. Some radiative heat losses at the tip and conductive losses upwards along the probe may have kept its tip at temperatures even lower than the flame tempera-

Author's personal copy

(a) (b) (c)

Fig. 2. Pictures of three ethyl benzene flames for which sampling data are reported herein: (a) $\phi_c = 1.68$, (b) $\phi_c = 1.74$ and (c) $\phi_c = 1.83$.

tures. Indeed, deterioration of the tip was never evident in these experiments.

2.1. Temperature measurements

Temperature measurements were conducted along the centerline of each flame at 15 axial locations with 178- and 76-μm bead diameter, Pt/Pt-10%Rh (type-S) *Omega* thermocouples, as described in detail in previous publications [1,2,13]. The thinner thermocouple ($d_{bead} = 76$ μm) was assumed to cause less disturbance of the flame and to possess better spatial resolution. Readings therefrom are reported herein, corrected for radiative losses by using a quasi-steady energy balance similar to that reported by McEnally et al. [14].

It should be mentioned here that bare (non-coated) S-type thermocouples were used for all temperature measurements in the manner of Wu et al. [15] and McEnally [14]. This decision was made as catalysis effects on thermocouple measurements in combustion environments are relatively ill-defined, both in terms of the magnitude of these effects and the conditions under which they are important. Common types of coatings are: silica-based coating, beryllium oxide/yttrium oxide ceramic, and alumina-based ceramic, but there have been issues with their fragility, toxicity, enhancement of the size of the bead, and stability at temperatures of 1900 K and above [31].

2.2. Sampling and analytical procedures

Probe sampling was performed along the axes of the three flames shown in Fig. 2. The small streaks in Fig. 2c are at the edges of the burner plug; lower temperatures encountered at the flame periphery have been reported to favor soot formation [16]. Small impurities and/or imperfections in the silicone sealant on that side of the burner may have induced localized gas flow distractions, causing faster cooling compared to other sections of the periphery. Sampling and temperature measurements were performed along the centerline of each flame; hence the results reported should not be affected by such small perturbations.

Sampling was conducted at the locations of 1, 3 and 7 mm above the burner. Condensed phase species were captured in the quartz wool, which was placed 1 cm upstream from the probe orifice. XAD-4 resin adsorbed semi-volatile PAH not captured by the glass wool. Samples of volatile gaseous hydrocarbons and fixed gases were collected by gas-tight 1 mL glass syringes downstream of the probe, see Fig. 1, and were injected into an HP 6890 Series GC with flame ionization and thermal conductivity detectors (GC-FID/TCD). O_2, CO, CO_2, C_1–C_4 and single-ring aromatic hydrocarbons were quantified with two parallel columns (100/120 Carbosieve S-II and HP-5 capillary column). Water was not accounted for, because of condensation on both the XAD resin and on the inner surfaces of the quartz probe. Therefore the mole fraction of water was not reported.

After the combustion experiments were completed, the quartz wool and XAD-4 resin samples were removed and placed in separate glass bottles with Teflon-lined caps, and stored in a refrigerator at 4 °C until analysis. Before extraction, a 50 μL internal standard mixture containing 100 μg each of naphthalene-*d8*, acenaphthene-*d10*, anthracene-*d10*, chrysene-*d12* and perylene-*d12* was directly added to the quartz wool as well as to the resins in each bottle. Blank combustion experiments in which the burner was operated in the presence of the XAD-4 and quartz wool but in the absence of fuel (hence in the absence of the flame), were performed. Target compounds that appeared in any of the blanks were appropriately quantified. A *Dionex* ASE 200 Accelerated Solvent Extractor was used for extracting the organic compounds from both the XAD-4 resins and the quartz wool. The XAD-4 resins were transferred to 33 mL extraction cells while the quartz wools were transferred to 11 mL extraction cells. The extraction cells were allowed to initially equilibrate at 40 °C in the ASE 200 system for one minute. The extraction cells were then filled with methylene chloride and allowed to thermally equilibrate at 40 °C; the cell was pressurized to 500 psi for a period of 15 min. Following the 15 min soak time the cells were each flushed with 80% of the cell volume with fresh methylene chloride and finally purged for 90 s with nitrogen. The methylene chloride extracts were collected in separate bottles for concentration. Two extraction cycles were used per cell. The total extraction time for the 2-cycle process was around 25 min. About 45 mL of methylene chloride were used for the XAD-4 resins while 20 mL were used for the extraction of the quartz wool. No more than 30 mL of XAD-4 resin could be placed within a 33 mL extraction cell due to the expansion of this resin in methylene chloride. The samples were concentrated under vacuum to a final volume of 10 mL for analysis by gas chromatography coupled to mass spectrometry (GC–MS).

The analytical studies were conducted in accordance with EPA Method 8270A as specified in SW846. The method was simplified to remove surrogate analysis procedures in the absence of potential matrix effects normally observed in environmentally obtained soil and water samples. Analytical data were reviewed based on the EPA's Volatile/Semivolatile Data Validation Functional Guidelines. Any analytical data that failed to meet those standards were rejected and the combustion experiments were repeated. The GC–MS system consisted of a Hewlett-Packard (HP) Model 6890 GC equipped with a HP Model 5973 mass selective detector. The GC–MS conditions and data reduction were described previously [17–19]. The instrument was tuned in accordance with EPA semivolatile criteria prior to the GC–MS analysis of each set of samples. The instrument passed initial and continuing calibration criteria. Each of the target compounds as well as the tentatively identified compounds were quantified using the appropriate deuterated internal standard. In a departure from the EPA method, the GC–MS system was run in the full scan mode and not in a single ion monitoring mode. This was done to ensure the identification, quantification and reporting of tentatively identified compounds. The use of the full scan mode does not significantly modify the method except to raise the lower reporting limit to about 1 μg of component per gram of fuel burned. Yields that are less than 1 μg/g are technically non-detects. Analysis of the combustion system blanks indicated the presence of xylenes, bis(2-ethylhexyl)-phthalate, and siloxanes in quantities sufficient to reject all positive results for these compounds in the combustion extracts.

The standard solutions containing 100 μg each of 5 characteristic standards were diluted to 10 mL, and were analyzed both as an instrument blank and to provide an indication of extrac-

Author's personal copy

tion efficiency for each of the internal standards. Samples with an extraction efficiency of less than 50% for any of the internal standards were repeated. The extraction recovery was in the range of 85–100%, which is in agreement with The National Functional Guidelines recommending a recovery of greater than 50% for the internal standards. In order to assess the reproducibility of the PAH analysis, triplicate analyses were performed. The source of the experimental error results from a combination of sampling, extraction, concentration and analysis techniques. The experimental procedure was kept consistent in all evaluations to ensure the validity of relative trends.

For fixed gases and light volatile hydrocarbons, the measured mole fractions were reported based on the areas on the output histograms of GC analysis. These areas are then calibrated against mixtures with known quantities of the species in question. The mass of each PAH, both condensed and vapor phases, was assessed using GC/MS analysis. Since the total volumetric flow rate through the probe, test duration time and molecular weights for each PAH are known, mole fractions were calculated using the ideal gas law. The details of the sampling/analysis method, and a discussion on experimental errors can be found elsewhere [1].

3. Results and discussion

3.1. Flame temperatures

The temperature profiles and the equivalence ratios are different for each flame. Nevertheless these flames have a similar faint orange glow, indicative of soot inception (Fig. 2). The temperature profiles of the three flames sampling were performed on, each at their soot onset limit, are presented in Fig. 3. These measurements were performed using a 76-μm-diameter thermocouple, and are corrected for radiative losses. Upon correction, all of the temperatures shifted to higher values in approximately proportional amounts; however, the relative values were not affected much. As the critical equivalence ratio increases from $\phi_c = 1.68$ to $\phi_c = 1.83$, the complete *measured* temperature profile, hence also the maximum temperature, shifts to higher temperatures. Similar temperature versus ϕ_c trends were also reported by Millikan [4], by Böhm et al. [7] and by Harris et al. [8], albeit with temperatures measured in those studies only at one location in the flames. The location and the magnitude of the maximum temperature, i.e., the location of the flame zone, changes for each condition as a result of the combination of the effects of equivalence ratio, the amount of diluent and the cold gas velocity of the flames. These parameters are listed in Table 1.

The precision of the thermocouples was investigated using a statistical technique. Individual temperature measurements in the post-flame zone were determined to be within ±8 K of the shown average values, using a 90% confidence interval. Close to the primary reaction zone the error was bigger. Due to steep temperature gradients therein, the measurements were extremely sensitive to the location of the thermocouple. Details of the temperature measurement technique and error analysis can be found in Refs. [1,13].

The reciprocals of the temperatures at 3, 7, 10 and 20 mm away from the surface of the burner, together with the maximum measured temperature in each flame regardless of its location, were plotted versus $\ln(\phi_c)$ in Fig. 4. The 10 and 20 mm locations match those for which Böhm et al. [7] and Olson and Madronich [6] reported their measurements, respectively. Harris et al. [8] showed that the reciprocals of maximum temperatures in the flames of aliphatic fuels fell on a straight line when plotted against $\ln(\phi_c)$. This was also confirmed for the aromatic ethylbenzene flames herein within experimental error. The threshold equivalence ratio and temperature can be correlated by $\ln\phi_c = A - \frac{B}{RT}$, where

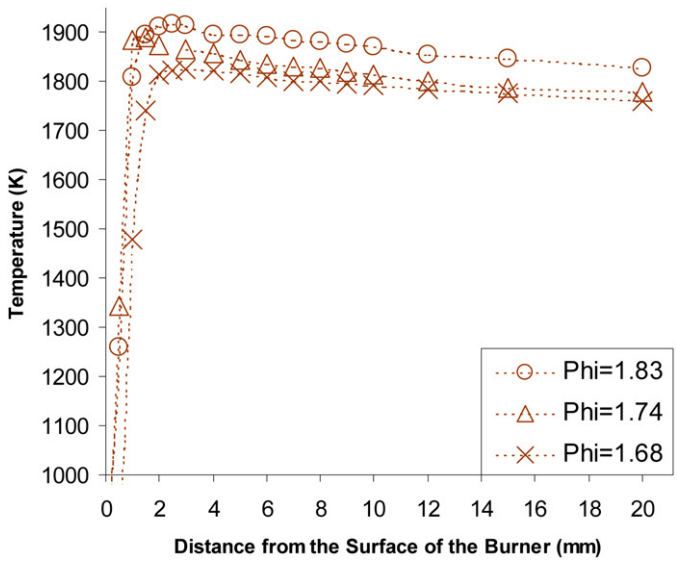

Fig. 3. Temperature profiles of the three flames in which sampling was conducted. These temperatures were measured with a 76-μm-diameter thermocouple and were corrected for radiative losses.

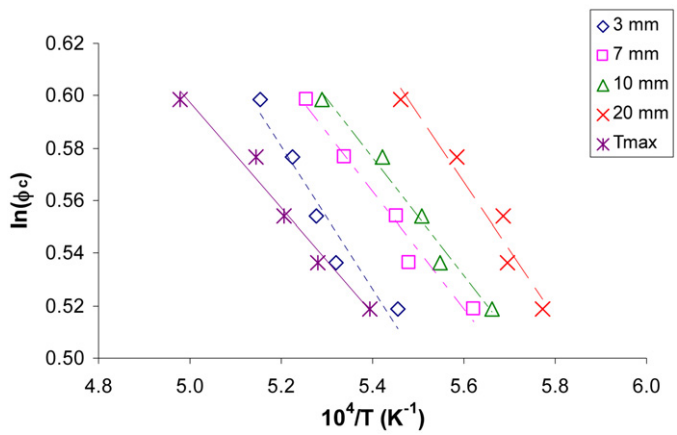

Fig. 4. Plot of $\ln(\phi_c)$ versus $1/T$ for four locations in the flame at different ϕ_c for all five atmospheric pressure ethylbenzene flames. The maximum recorded temperature of each flame, regardless of axial location, is also included.

A and B are positive constants and R is the universal gas constant. The above relationship is similar to the Arrhenius equation, $k = A \times \exp(-E_a/RT)$, describing the temperature dependence of the rate constant k with E_a being the activation energy. The validity of this relationship has been shown by different authors covering a large temperature range within the limits of a stable flame. A possible explanation could be that increasing temperature accelerates reactions leading to the oxidation of soot and, particularly, its precursors. Therefore, sooting threshold and oxidation reactions show both an Arrhenius-type behavior. According to Harris et al. [8], $A \sim 1.85$ for their C_2H_4/air flame and $A \sim 1.55$ for their C_2H_4/O_2 flame, whereas $B \sim 18$ kJ/mol for C_2H_4/air flames investigated and $B \sim 12$ kJ/mol for C_2H_4/O_2 flames investigated. Takahashi and Glassman [20] changed the temperatures of their flames through changing the nitrogen flow rate and they calculated the change in adiabatic flame temperature. According to that, they found that $B \sim 13$ kJ/mol for nearly all aliphatics and $B \sim 25$ kJ/mol for some aromatic fuels. In the case of ethylbenzene flames, and in the range of conditions examined herein, the following values were deduced: $A = 1.61$ and $B = 16.8$ kJ/mol, both of which are in the range of the aforementioned values.

Author's personal copy

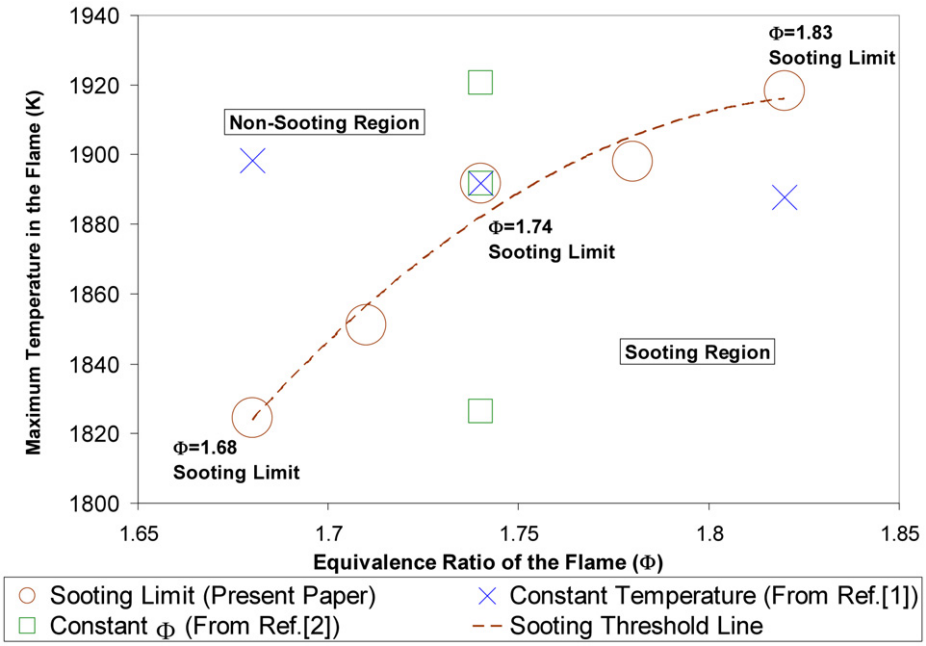

Fig. 5. Maximum temperatures (corrected for radiative losses) of atmospheric pressure ethylbenzene flames at or near their soot onset limit, either reported herein or in recent publications [1,2].

The two-dimensional map depicted in Fig. 5 defines the location of the flames studied in the present work (shown with the symbol ○) in the ϕ_c–T_{max} parameter space. Also included in this map are locations of flames, studied in previous work, where the equivalence ratio was varied while keeping the temperature constant [1] (represented with the symbol ×), or the temperature was varied while keeping the equivalence ratio constant [2] (represented with the symbol □).

3.2. Fuel consumption, fixed gases and light hydrocarbon concentrations

The mole fractions of ethylbenzene (the fuel of these flames) along the flame axis are depicted in the first entry of Fig. 6, where the symbols represent experimental measurements and the lines represent predictions of a detailed chemical kinetic model, discussed in an ensuing section. The fuel plot is followed by the oxygen consumption plot.

The oxygen concentrations were similar in all of the flames. Most of the initial O_2 (see values in Table 1) was consumed close to the burner surface reaching mole fractions in the range of 0.83–0.86% at 1 mm downstream from the burner and 0.65–0.72% at 7 mm. Although most fixed gases and light hydrocarbons had generally similar values in these three flames, especially in the post-combustion region, the CO mole fractions were very dissimilar. The hotter and richer flames produced considerably more CO; values increased from 9.8 to 17% in the $\phi_c = 1.68$ flame; from 11.2 to 18.8% in the $\phi_c = 1.74$ flame; and from 14.5 to 22% in the $\phi_c = 1.83$ flame. CO_2 mole fractions were initially in the 8.2–11.3% range; thereafter they converged to 7.5% in the post-flame zones of all flames.

The mole fractions of most of the light volatile hydrocarbons increased initially, reaching higher concentrations at 3 mm, possibly peaking around that point (the end of primary oxidation zone) and thereafter they were partially consumed downstream in the flame. Light hydrocarbons and small aromatics such as acetylene and benzene are likely soot precursors [21–24]. The concentrations of acetylene and benzene in different flames in Fig. 6 ranked inversely proportional to the equivalence ratio and hence the maximum temperature of the flames. Therefore, a similar trend is expected for multi-ring PAH and soot and has been confirmed in the recent study on ethylbenzene flames [1].

3.3. Polycyclic aromatic hydrocarbon (PAH) concentrations

Mole fractions of major semi-volatile polycyclic aromatic hydrocarbons (PAH) as well as of total PAH are shown in Fig. 6. Please note that, since the major fixed gases (CO, CO_2, O_2) were detected in the same order of magnitude at each sampling location, their plots were presented in linear scale in Fig. 6. The hydrocarbons, on the other hand, spanned more than one order of magnitude; hence their plots were presented in logarithmic scale. The most abundant PAH was naphthalene followed by indene and acenaphthylene. Found in comparable concentrations was phenol, an oxygenated aromatic hydrocarbon.

The PAH concentrations of all three flames experienced decreasing trends along their axes. The differences in PAH concentration of these flames seemed to be more pronounced in the 1–3 mm region. This is expected, as this region encompasses the primary reaction zone, i.e., the flame front. Thereafter, concentrations tend to converge towards each other at 7 mm in the post-flame zone. This trend was also observed in previous work, where the equivalence ratio was kept constant and the temperature was varied to induce either sooting or non-sooting conditions [2]. Some PAH such as indene, fluoranthene and pyrene, were consumed in the post-flame zone to values below the detection limit.

A possible explanation as to why the species converged at 7 mm from the surface of the burner was presented in previous work [2]. Oxidation reactions via OH and O radicals are likely to consume PAH in the hotter flames, while soot formation reactions via soot precursor free radicals such as propargyl are more likely to consume PAH in the cooler flames. These different mechanisms bring the PAH concentrations of the three flames close to one another, under these conditions coincidentally around the 7 mm point. The argument on enhanced oxidation reactions is supported by the model's predictions when comparing the OH maximum mole fraction in the hottest flame (1.3×10^{-4}) to that in the coolest flame (9.5×10^{-5}). Not only is the maximum OH concen-

Author's personal copy

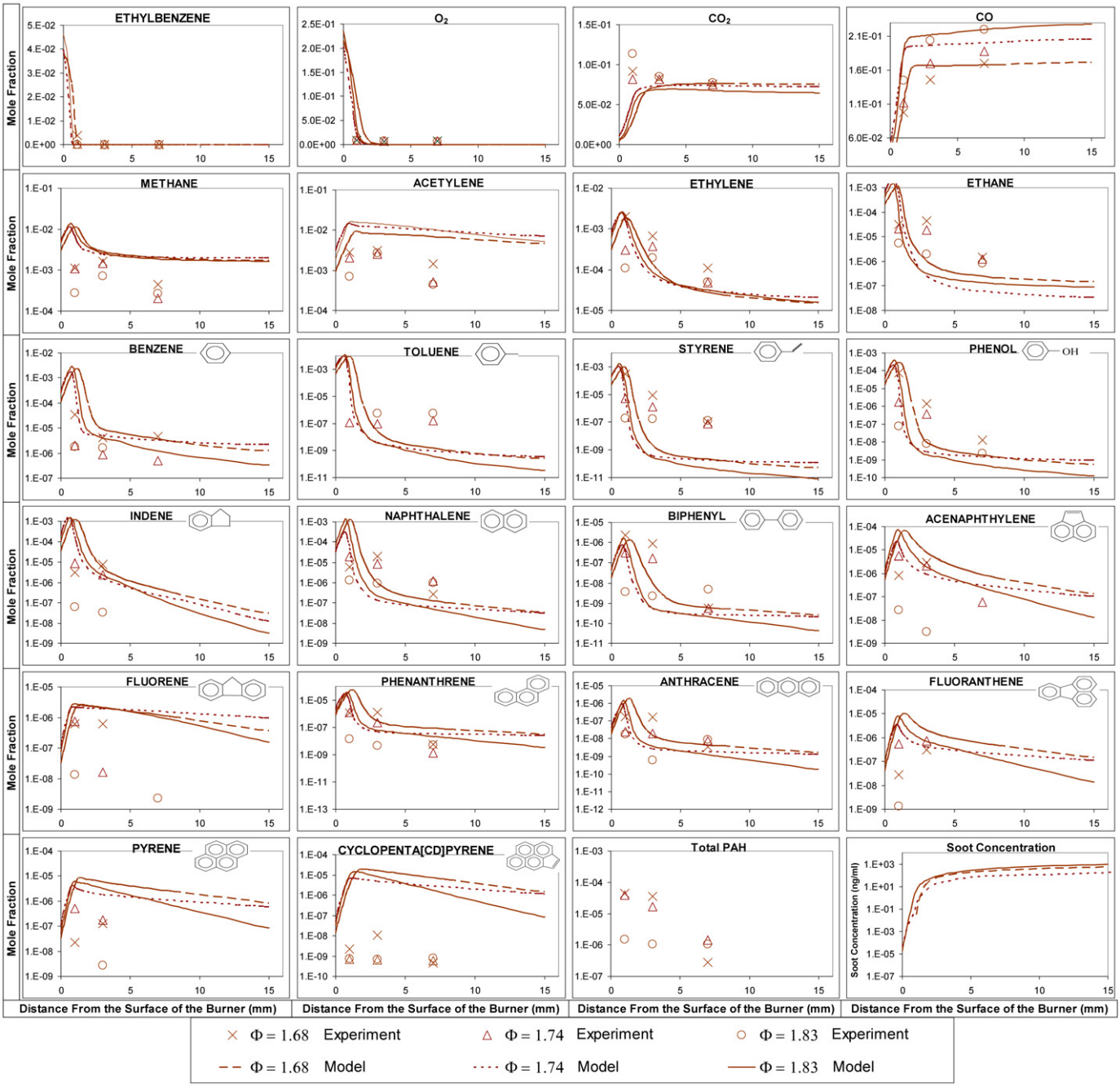

Fig. 6. Concentrations of fixed gases, light hydrocarbons and PAH for three flames ($\phi_c = 1.68$, $\phi_c = 1.74$ and $\phi_c = 1.83$) at their soot onset limit. Ethylbenzene, CO, CO_2 and O_2 plots are in linear scale, the other plots are in logarithmic scale.

tration higher in the hotter flame but, also, the entire OH profile therein is higher than that of the coolest flame throughout their post flame zones.

A major observation on Fig. 6 is that PAH concentrations in the coolest $\phi_c = 1.68$ flame are generally 1–2 orders of magnitude higher than those in the hottest $\phi_c = 1.83$ flame, with the concentrations of the $\phi_c = 1.74$ flame generally falling in between. This fact, along with the widely accepted assumption, that multi-ring PAH are the predominant soot precursors supports the observations of Böhm et al. [7], who found that flames at relatively high temperatures have lower soot loadings compared to cooler flames at their visual sooting limit.

In the coolest $\phi_c = 1.68$ flame 48 PAH were identified and quantified in the primary reaction zone (1–3 mm above the surface of the burner), whereas only 11 were detected in the post-flame region. Most species were more abundantly collected in the gaseous phase (i.e., on the XAD resin), the exceptions being phenol, phenanthrene and cyclopenta[cd]pyrene at the highest sampling point (7 mm above the surface of the burner).

In the intermediate-temperature $\phi_c = 1.74$ flame a total of 30 PAH were quantified at 1–3 mm. Again most of the detected species were more abundant in the gaseous phase except phenanthrene, methylphenanthrenes, cyclopenta[cd]pyrene and benz[a]anthracene. At the highest sampling point 20 compounds were detected.

In the hottest $\phi_c = 1.83$ flame only 23 PAH were detected and quantified at 1–3 mm, out of which 18 were also detected at the highest sampling point. Once again most of the com-

Author's personal copy

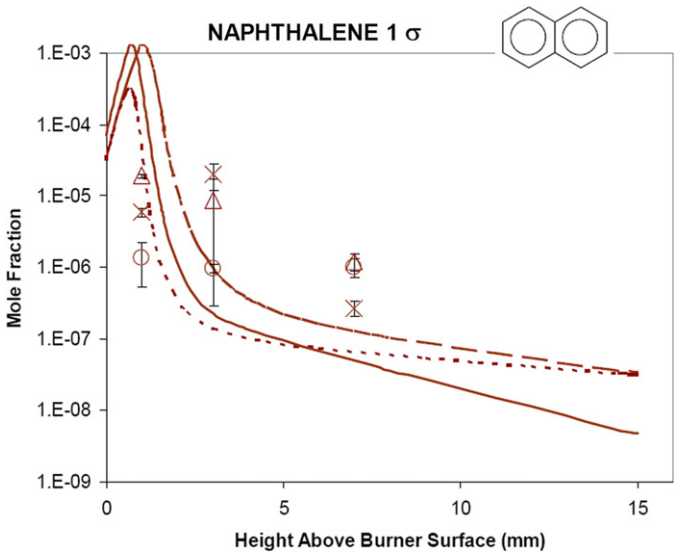

Fig. 7. Naphthalene mole fraction graph with one standard deviation (σ) bars included.

pounds were collected in the gaseous phase. The exceptions being phenol, 2,3-dihydro-1H-indene-1-one, fluorene, phenanthrene, 3-methylphenanthrene, 9,10-anthracenedione, cyclopenta[cd]pyrene, benz[a]anthracene, and benzo[a]fluoranthene at the highest sampling point.

To better assess the repeatability and reproducibility of the measurements of the flame composition, representative species were selected and statistically analyzed. All measurements in this work were conducted in triplicate, and the means and standard deviations were calculated for each species. Using the mean and standard deviation, 90% confidence intervals were created for CO, acetylene, and naphthalene. These confidence intervals were then used to generate error bars for the select species. It was discovered that at the 1 mm sampling point the ranges for CO and acetylene were very broad and the error bars of different flames overlapped. This showed that the repeatability of the measurements at 1 mm above the burner surface were not very good, most likely because of steep temperature gradients in this region and the sensitivity of this technique to local conditions immediate to the probe tip. This is not surprising due to the proximity of this sampling point to the primary reaction zone. However, for the 3 mm and 7 mm points the ranges were much narrower (for instance, at 3 mm from the surface of the burner, the mean mole fraction of acetylene was 2.55e–3 with a confidence interval of ±2.83e–4), and lead to much smaller portions of error bars overlapping, though overlapping still occurred. Naphthalene showed large errors in the vicinity of the primary reaction zone (3 mm sampling point). Specifically, the $\phi_c = 1.74$ flame error bars overlapped those of the other two flames (i.e. $\phi_c = 1.68$ and $\phi_c = 1.83$) at the 3 mm sampling point. However, the error bars for the $\phi_c = 1.68$ and $\phi_c = 1.83$ flames did not overlap each other at this sampling point. The 7 mm sampling point had the narrowest error bars for all flames, with overlapping only occurring due to the close proximity of the $\phi_c = 1.74$ and $\phi_c = 1.83$ flames. As an example of this analysis the mean points with error bars corresponding to one standard deviation (1σ) for the most predominant PAH (i.e., naphthalene) are shown in Fig. 7.

3.4. Soot concentrations

The common characteristic of these flames at the soot onset limit is that they all looked similar, i.e. they all had a similar faint orange glow (Fig. 2). While the human eye is not necessarily the best judge of the contribution of soot, it has been shown before that the visual determination of soot onset limit is reproducible to within 2% by different observers [6,7]. For a faint orange glow to be visible in all these flames (see Fig. 2) some soot, no matter how little, must have been present. Nevertheless, no soot was evident in the collected quartz wool samples either gravimetrically or upon examination with optical microscopy. Thus, soot particle concentrations in these flames were too low to be reliably measured with the techniques used herein. As additional soot detection techniques were not available in this laboratory, the question as to whether these soot-threshold flames had the same or different soot concentrations could not be answered directly. However, two inferences can be offered; one is based on past findings on the radiating properties of flames, and the other on the measured concentrations of soot precursors.

(i) It has been demonstrated in the past by H.C. Hottel [25,26] that the soot radiating properties depend almost completely on the product of path length, L, and mole fraction, S, of soot in the gas, i.e., on the moles of carbon per mole of gas in which it is suspended, and interestingly *not* (or, at least, hardly at all) on gas temperature.

This may be surprising to the reader, since the monochromatic emissivity in optically thin and isothermal flames due to their soot content *does* depend on temperature T (K), and is given by [25,27]:

$$\varepsilon_\lambda = 1 - \exp(-0.526SL/\lambda T).$$

Then the total emissivity, due to soot can be calculated from:

$$\varepsilon_{\text{total}} = \int_0^\infty E_\lambda \varepsilon_\lambda \, d\lambda / \sigma T^4,$$

where the monochromatic emissive power of a blackbody, E_λ, is given by Planck's law and σ is Stefan–Boltzmann's constant. Following a brief but rather intricate solution, Hottel showed that the total emissivity due to soot *does not* depend on temperature and is given by:

$$\varepsilon_{\text{total}} = 1 - (1 + 34.5SL)^{-4}.$$

Thus, for instance, doubling the absolute temperature of a flame in which the soot mole fraction and path length are constant will, at constant pressure, halve the concentration of soot but not change the total soot emissivity. Hottel called this generalization a great simplifier [25,26]. The soot concentration reduction is due to the fact that soot concentration is a function of the gas volume, which changes with respect to temperature.

In the three visually similar flames of this work the total emissivities are presumably the same, at least in the visible spectrum of light. Hence as L is the same, S must also be the same. Therefore, as the temperature decreases from the $\phi_c = 1.83$ flame to the $\phi_c = 1.68$ flame, the soot concentration must increase accordingly. This argument was substantiated by Böhm et al. [7], who reported higher soot loadings in cooler flames (1400 K) with the same luminosity (total emissivity) as hotter flames (1900 K).

(ii) In support of the above arguments, it was observed that the number and the concentrations of PAH species detected in the reaction zone of the coolest $\phi_c = 1.68$ flame were the highest, followed by those in the intermediate-temperature $\phi_c = 1.74$ flame, and then by those in the hottest $\phi_c = 1.83$ flame. This fact also suggests that the coolest flame also had a higher soot concentration than either the intermediate-temperature or the hottest flame, even though all flames were visually similar.

3.5. Kinetic model

A kinetic model describing the formation and consumption of PAH and carbonaceous material (soot) has been developed, successfully tested with a premixed benzene low-pressure flame [28]

Author's personal copy

and extended to the premixed combustion of ethylbenzene and ethanol at atmospheric pressure [29]. Numerical predictions were compared to data and observations qualitatively assessed. All model computations were conducted with the *Premix* code of the *Chemkin* software package [30] using the experimental temperature profile. Further details of the model can be found elsewhere [1,28,29]. The reaction mechanism used, consisted of 335 species and 8086 reactions and, together with thermodynamic property and transport data files is provided along with this manuscript as supplemental material, appearing at the web site of this journal.

For all the flames, the model predicted steadily declining mole fractions of oxygen throughout the entire flame profile (Fig. 6). The CO and CO_2 experienced rapidly increasing trends in the first 1–2 mm (primary reaction zone) of the flame and then leveled off. The model predicted a sharp increase for all the hydrocarbon species in the first 1–2 mm of the flame where they reached a peak and then decreased. The light hydrocarbons and PAH species with two- or three-rings undergo a sharp decline after the primary reaction zone until 3–4 mm where they level off and decrease mildly thereafter. The four-ring and higher species undergo a gradual decline from their peak to the end of the profile. Most species profiles in the hottest $\phi_c = 1.83$ flame initially experienced a maximum and then rapid consumption, presumably predominantly through oxidation reactions involving radicals, as the formation of much soot was not evident.

The model predicted the O_2 mole fractions reasonably well at the 1 mm axial distance above the burner, but underpredicted them in the post flame zone. CO and CO_2 mole fractions were predicted with considerable fidelity. The model overpredicted the methane, acetylene, pyrene, cyclopenta[cd]pyrene, and benzo[ghi]fluoranthene. It experienced partial success in predicting benzene, styrene, toluene, indene, acenaphthylene, fluorene and fluoranthene. In these cases some experimental points agreed with the model, whereas others were well above or bellow what was predicted. Mole fractions of ethylene, ethane, naphthalene, biphenyl, phenanthrene, anthracene, and phenol were predicted with considerable fidelity. The model shows that the concentrations of light hydrocarbons and PAH for all the flames converge and sometimes cross at a point in the post flame region usually in the vicinity of 7 mm. This is in good agreement with trends in the experimentally determined concentrations which showed similar converging trends at 7 mm from the surface of the burner.

The model predicted soot in the flames, but it did not predict much variation among the soot concentration profiles, as can be seen in the last graph in Fig. 6. The predicted soot concentrations in the post flame region were possibly above reported optical detection limits [2,7]. However, the model does not include the oxidation of some PAH and nascent soot particles, which is an important consideration at high temperatures. Therefore, it is quite likely that the soot concentration profiles are overestimated, especially in the hottest flame (i.e., the $\phi_c = 1.83$ flame). This calls for additional work in this area, although the model predicted soot profiles in the past, which matched the experimental profiles of highly sooting flames. For instance, the modeling of a strongly sooting ethylbenzene flame [29] has showed a significant increase in PAH concentrations, in agreement with the experimental data. Lower concentrations of PAH and the absence of soot in a fuel-rich ethanol flame have also been correctly reproduced by the model. Details of the reaction mechanism and pathways involved in PAH and soot formation have been discussed previously [1,2,29].

4. Conclusions

Five one-dimensional, atmospheric-pressure, premixed ethylbenzene flames at their sooting limit were stabilized over a flat-flame burner. Axial temperature profiles were determined via thermocouple measurements. Concentrations of fixed gases, light hydrocarbons, and polycyclic aromatic hydrocarbons (PAH) were determined in three of these flames ($\phi_c = 1.68$, $\phi_c = 1.74$ and $\phi_c = 1.83$) via probe sampling, followed by GC analysis.

Axial temperature profiles throughout each flame were observed to be progressively more elevated at higher critical equivalence ratios. The reciprocals of the maximum temperatures inside each flame, regardless of their location, were shown to fall on a straight line when plotted versus $\ln(\phi_c)$, as it was also previously shown by Harris et al. [8] for flames of other fuels.

CO mole fractions were dissimilar, increasing in the order of increasing equivalence ratio and increasing flame temperature, a trend also observed earlier in flames of fixed equivalence ratio but increasing temperature [2]. This difference may be due to faster oxidation kinetics, as compared to soot-formation kinetics, at higher temperatures. The mole fractions of most light hydrocarbons increased in the initial stages of combustion, peaked along the flame and then decreased, presumably because of surface reactions with nascent soot particles of increasing size. Experimentally detected PAH experienced declining mole fractions along the flames. Abundance of both light hydrocarbon and PAH species was inversely proportional to ϕ and, thus, to flame temperatures in these flames. The hotter and fuel-richer flame had the lowest concentration of light hydrocarbons and PAH; it also had the fewest PAH species detected in the reaction zone. This is in good agreement with a recent study [1], which indicated that the concentrations of higher molecular weight PAH (3–4 rings) and the soot concentrations would follow the same trend, i.e. the hotter/richer flame will most likely have lower soot concentration at its soot onset limit compared to the cooler, leaner flames. This was also observed by the experimental work of Böhm et al. [7] and was supported by flame radiation arguments, based on the findings of Hottel [25,26]. Comparisons with a kinetic model were consistent for most fixed gases, volatile and semi-volatile hydrocarbons, however, the computed soot concentrations were at or above possible optical detection limits.

Supplementary material

The online version of this article contains additional supplementary material.

Please visit DOI: 10.1016/j.combustflame.2008.11.013.

References

[1] A. Ergut, Y.A. Levendis, H. Richter, J.B. Howard, J. Carlson, Combust. Flame 151 (2007) 173–195.
[2] A. Ergut, R.J. Therrien, Y.A. Levendis, H. Richter, J.B. Howard, J. Carlson, Combust. Flame 155 (2008) 232–246.
[3] J.C. Street, A. Thomas, Fuel 34 (1955) 4.
[4] R.C. Millikan, J. Phys. Chem. 66 (1962) 794.
[5] J.J. Macfarlane, F.H. Holderness, F.S.E. Whitchers, Combust. Flame 8 (1964) 215–229.
[6] D.B. Olson, S. Madronich, Combust. Flame 60 (1985) 203–213.
[7] H. Böhm, D. Hesse, H. Jander, B. Luers, J. Pietscher, H.G.G. Wagner, M. Weiss, Proc. Combust. Inst. 22 (1988) 403–411.
[8] M.M. Harris, G.B. King, N.M. Laurendeau, Combust. Flame 64 (1986) 99–112.
[9] A. Ciajolo, A. D'Anna, R. Barbella, A. Tregrossi, A. Violi, Proc. Combust. Inst. 26 (1996) 2327–2333.
[10] P. Markatou, H. Wang, M. Frenklach, Combust. Flame 93 (1993) 467.
[11] A. Ergut, Ph.D. thesis, Northeastern University, Boston, MA, April 2007.
[12] CRC Handbook of Chemistry and Physics, 65th ed., CRC Press, Boca Raton, FL, 1985.
[13] A. Ergut, Y. Levendis, in: Proc. of ASME International Mechanical Eng. Congress and Expo. (IMECE2005), Orlando, FL, 2005.
[14] C.S. McEnally, Ü.O. Köylü, L.D. Pfefferle, D.E. Rosner, Combust. Flame 109 (1997) 701–720.
[15] J. Wu, K.H. Song, T. Litzinger, S.-Y. Lee, R. Santoro, M. Linevsky, M. Colket, D. Liscinsky, Combust. Flame 144 (2006) 675–687.

Author's personal copy

[16] M. Bachmann, W. Wiese, K.-H. Homann, Combust. Flame 101 (1995) 548–550.
[17] T. Panagiotou, Y.A. Levendis, Combust. Flame 99 (1994) 53–74.
[18] J. Wang, Y.A. Levendis, H. Richter, J.B. Howard, J. Carlson, Environ. Sci. Technol. 35 (2001) 3541–3552.
[19] Z. Wang, J. Wang, H. Richter, J.B. Howard, J. Carlson, Y.A. Levendis, Energy Fuels 17 (2003) 999–1013.
[20] F. Takahashi, I. Glassman, Combust. Sci. Technol. 37 (1984) 1.
[21] I. Glassman, Proc. Combust. Inst. 22 (1988) 295–311.
[22] H. Richter, J.B. Howard, Prog. Energy Combust. Sci. 26 (2000) 565–608.
[23] M. Frenklach, Phys. Chem. Chem. Phys. 4 (2002) 2028–2037.
[24] C.S. McEnally, L.D. Pfefferle, B. Atakan, K. Kohse-Hoinghaus, Prog. Energy Combust. Sci. 32 (2006) 247–294.
[25] H.C. Hottel, AIChE Symp. Ser. 82 (249) (1986) 1–12.
[26] H.C. Hottel, personal communication to YAL, 1992.
[27] W.L. Flower, Combust. Sci. Technol. 33 (1983) 17–33.
[28] H. Richter, S. Granata, W.H. Green, J.B. Howard, Proc. Combust. Inst. 30 (2005) 1397–1405.
[29] A. Ergut, S. Granata, J. Jordan, J. Carlson, J.B. Howard, H. Richter, Y.A. Levendis, Combust. Flame 144 (2006) 757–772.
[30] R.J. Kee, F.M. Rupley, J.A. Miller, M.E. Coltrin, J.F. Grcar, E. Meeks, H.K. Moffat, A.E. Lutz, G. Dixon-Lewis, M.D. Smooke, J. Warnatz, G.H. Evans, R.S. Larson, R.E. Mitchell, L.R. Petzold, W.C. Reynolds, M. Caracotsios, W.E. Stewart, P. Glarborg, C. Wang, C.L. McLellan, O. Adigun, W.G. Houf, C.P. Chou, S.F. Miller, P. Ho, P.D. Young, D.J. Young, CHEMKIN Release, 4.0.2, Reaction Design, San Diego, CA, 2005.
[31] K.A. Burton, H.D. Ladouceur, J.W. Fleming, Combust. Sci. Technol. 81 (1992) 141–145.